Pergamon

Int. J. Heat Mass Transfer. Vol. 39, No. 6, pp. 1149–1156, 1996

0017-9310/96 $15.00 + 0.00

0017-9310(95)00212-X

Measurement and use of bi-directional reflectance

JOSEPH R. ZAWORSKI,† JAMES R. WELTY† and M. KEVIN DROST‡

† Department of Mechanical Engineering, Oregon State University, Corvallis, OR 97331-6001, U.S.A.
‡ Pacific Northwest Laboratory,§ Richland, WA 99352, U.S.A.

(*Received* 18 *April* 1994 *and in final form* 20 *June* 1995)

Abstract—Bi-directional reflectance is a fundamental surface property that has received a great deal of attention, particularly during the early years of the space program. Although the value of using accurate surface property data has always been recognized, bi-directional reflectance information is rarely used because of the sheer volume of data involved. Now, with powerful workstations readily available, large Monte Carlo codes can be run very quickly and full advantage can be taken of the detailed surface property description provided by bi-directional reflectance data. This paper provides a detailed description of a simple, compact, flexible apparatus for measuring bi-directional reflectance and a review of measurement considerations.

INTRODUCTION

Bi-directional reflectance is a material surface property that is fundamental to many types of radiative transfer calculations. An indication of the importance of this property is given by the fact that there are literally hundreds of archival publications describing methods for analytically estimating reflectivity, explaining and modeling the effects of variables such as surface roughness and polarization, and describing the results of experimental measurement of reflectance properties (see for example [1, 2]). Although analytical methods have been developed for predicting surface properties [3, 4], their application is often of limited value for use with materials that have been abraded, oxidized, or which have had some other action change their surface properties. In these cases, experimental data are required.

The motivation for this work is the need for accurate characterization of surface properties for the validation of a Monte Carlo model. The specific application for this model is the study of radiative transfer through an array of fixed discrete surfaces. In this application, the surface properties of individual elements, in particular their bi-directional reflectance, play major roles in determining the uncertainty of results because each photon bundle may have many surface interactions prior to leaving the array.

To the best of our knowledge, there have been no Monte Carlo codes reported that make full use of bi-directional reflectance data. Virtually all codes using reflectance data model the reflectance as the sum of a specular and a diffuse component. To arrive at this model from a set of bi-directional data, it is common to assume at least one, and sometimes two axes of symmetry for the data. The common assumption is that of azimuthal symmetry about the incident beam, i.e. reflectance properties do not change with respect to the azimuth angle of the incident beam, only with respect to the incident beam polar angle. This is a reasonable assumption for many types of surfaces that are smooth either because the surface has been carefully prepared (as in a laboratory), or because of a filling process such as painting, which naturally results in a smooth surface. However, this assumption of azimuthal symmetry does not seem reasonable for many common engineering materials containing non-random surface features: materials such as brush-finished stainless steel, extruded aluminum, any material that has been machined, or materials that have been sanded in one direction. For these materials, a full set of bi-directional reflectance data is required to accurately describe the material reflectance properties. It is for this reason that the bi-directional reflectometer described in this paper was developed.

In the sections that follow, a detailed description of the bi-directional reflectometer, some measurement considerations, operation, and some example data are presented. The apparatus is described in detail including its construction, as well as the alignment and calibration procedures, operational procedures, and a discussion of uncertainty.

NOMENCLATURE AND DEFINITIONS

The nomenclature listed above follows convention [5, 6]. The word reflectivity is reserved for describing an optically smooth uncontaminated surface; reflectance is used with measured properties where there are no constraints on surface conditions. Geometric

§ Operated for the U.S. Department of Energy by Battelle Memorial Institute under contract DE-AC06-76RLO 1830.

NOMENCLATURE

A	surface area [mm^2]
i	intensity [W mm^{-2} sr^{-1}]
q	energy flux [W mm^{-2}]
r	radius [mm]
V	[V].

Greek symbols

θ	polar angle (measured from normal to the surface)
ρ	reflectivity (no units)
ϕ	azimuthal angle.

Superscripts

$''$	bidirectional
$'$	directional.

Subscripts

o	incident from a collimated beam
λ	spectral
i	incident
r	reflected.

descriptions are based on a reference system that is attached to the surface of interest; the incident beam and the reflected beam directions are defined by two angles each (see inset, Fig. 2). The bi-directional spectral reflectance (with a collimated source) is then defined as:

$$\rho''_\lambda(\theta_i, \phi_i, \theta_r, \phi_r) = \frac{i_{r,\lambda}(\theta_i, \phi_i, \theta_r, \phi_r)}{q_o \cos(\theta_i)}. \quad (1)$$

Note that both the figure and the equation for reflectance (1) have been selected for the case of a collimated incident beam. For this case the intensity at the surface of interest need be adjusted by the incident polar angle only; the solid angle adjustment usually included in the denominator is omitted. Examination of this definition reveals that the reflectance defined in this way can be greater than one. For this reason, the name bi-directional reflectance distribution function (BRDF) is usually used for this quantity. Finally, note also that bi-directional reflectance is a ratio of intensities. This is important because the output of a sensor will be either voltage or current. Since the bi-directional reflectance is a ratio of intensities, it is also a ratio of the incident and reflected sensor outputs. In other words, there is no need to calibrate sensors to measure intensity on an absolute basis. This will result in a much easier measurement scheme and will decrease the overall experimental uncertainty.

In addition to bi-directional spectral reflectance, the directional-hemispherical spectral reflectance is also a useful quantity. The integral form is obtained by multiplying the bi-directional reflectance by the area of the sensor and the solid angle of the reflected beam and then integrating over the entire hemisphere [5].

$$\rho'_\lambda(\theta_i, \phi_i) = \frac{\int_{2\pi} i''_{r,\lambda}(\theta_i, \phi_i, \theta_r, \phi_r) \cos\theta_r \, d\omega_r}{q_o \cos\theta_i}$$

$$\approx \sum_{i=1}^{n} \rho''_\lambda(\theta_i, \phi_i, \theta_r, \phi_r)^* \Delta\omega_r. \quad (2)$$

This quantity is useful because approximation of the integral with a summation of bi-directional data for n solid angles over the hemisphere will allow comparison with the results from an integrating sphere.

DETAILS OF THE REFLECTOMETER

As implied in the introduction, there have been numerous devices built for measuring bi-directional reflectance [1, 7–10]. In nearly all previous designs, both the radiation source and the sensing apparatus have been large. Since full hemispheric coverage for BRDF requires that either the source, sensor, or both move around the sample, devices with large sources and sensors have typically been limited to in-plane scanning. In addition, calibration of the source–sensor system usually involves special mirrors not used in the actual BRDF measurements.

The design of the reflectometer used in this project began with an apparatus based on the one developed by Hsia [9]. After much experimentation and redesign, it evolved to a completely new apparatus based in part on the approach used by De Silva [7]. The features that make this reflectometer particularly useful are (1) complete hemispherical coverage with the exception of (a) a small cone around the incident beam and (b) a small band at the base of the hemisphere, where the polar angles approach 0° and 90°, respectively; (2) high sensitivity for use with low reflectance materials; (3) the ability to easily use virtually any type of source for the incident beam; (4) direct reading of the four angles that define incident and reflected directions and (5) the ability to temporarily position the sample out of the way so that the sensor can be aligned directly with the incident beam for calibration and direct measurement of incident beam intensity.

The entire apparatus is shown schematically in Fig. 1 and details of the goniometer are shown in Fig. 2. The reflectometer can be considered in terms of three major subsystems: the source, the goniometer, and the detection system. In the course of subsequent descriptions, note that the reference coordinate system is located on the sample of interest. The incident beam is fixed, and the sample–sensor apparatus rotates around the point at which the incident beam intersects the front plane of the sample.

The source

One of the advantages of the physical arrangement of this apparatus is that the source is fixed in position;

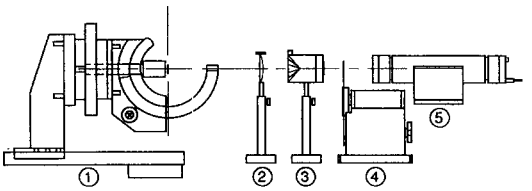

Fig. 1. A schematic representation of the apparatus: (1) goniometer; (2) collimating lens; (3) spatial filter; (4) chopper- and (5) He–Ne laser. Not shown are the silicon photodiode sensor (mounted on the goniometer arm) and the lock-in amplifier and computer used to measure the sensor output.

bi-directional measurements over nearly the entire hemisphere are accomplished by moving only the sample and the sensor. This means that virtually any source can be used because there are no size, weight, or orientation constraints as might exist if the source was a moving part of the goniometer system. In fact, a 0.5 mW He–Ne laser, a 5 mW He–Ne laser and a quartz–tungsten halogen (QTH) source have already been used with this apparatus and a 2 W argon laser is mounted on the same table and available if needed. The source used for the work reported in this paper was a 5 mW He–Ne laser operating at 632.8 nm.

Three source configurations were evaluated for use with this apparatus: a non-uniform beam smaller than the sample, a uniform beam larger than the sample, and a uniform beam of the same diameter as the sample. In all cases, the beam was collimated and monochromatic and, except for some early experimentation with a QTH source, all work was done with a He–Ne laser. Laser output was used directly for the narrow band beam. This beam had an output of either 0.5 or 5 mW depending on which laser was used, the wavelength was 632.8 nm, the beam diameter was on the order of 1 mm, and the measured beam intensity distribution was approximately gaussian. For the large-diameter beam, a spatial filter consisting of a focusing lens, a 0.03 μm diameter pinhole, and appropriate positioning verniers were used to expand the beam. An additional lens was used to recollimate the center portion of the beam to provide a monochromatic, collimated beam of approximately 25 mm in diameter with a measured beam intensity distribution that was uniform. Only the higher power laser (5 mW) was used for the wide beam. The same

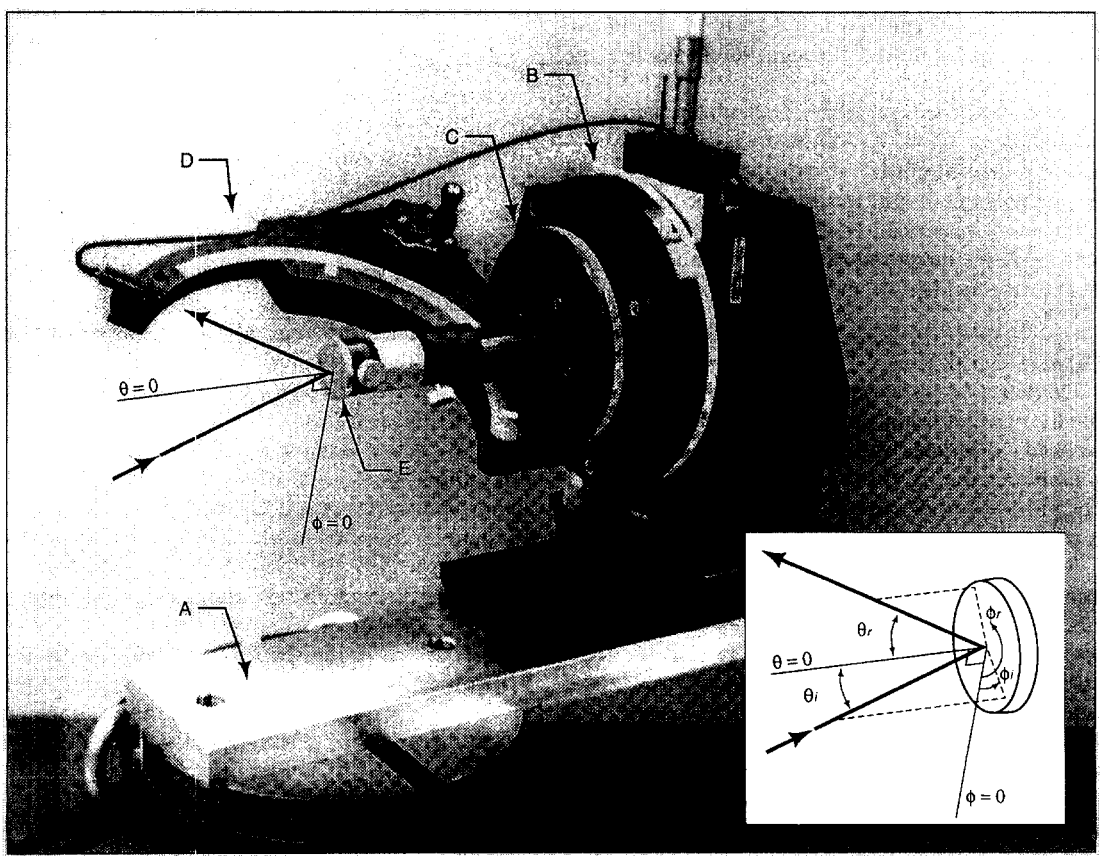

Fig. 2. A photograph of the goniometer. The path of the incident beam to the sample and a beam reflected to the sensor are shown. The rotational stage (A) and the goniometer arm (D) are used to vary the incident and reflected polar angles, respectively. The rotational stages (B) and (C) are used to change the incident and reflected azimuthal angles.

arrangement was used with a mask when the beam diameter was limited to the sample diameter.

The goniometer

The incident beam is parallel to the goniometer base and impinges directly on a sample mounted in the goniometer apparatus (Fig. 2). The entire sample–sensor apparatus sits on a rotation stage (A), the surface of which is parallel to the optical table on which it is mounted; changing the orientation of the apparatus with this stage changes the incident beam polar angle. Mounted on stage (A) but oriented vertically is another rotation stage (B), the sample (E) is mounted directly to this stage so that rotating (B) changes the azimuth angle for the incident beam.

This arrangement effectively allows the angles defining the reflected beam direction to remain unchanged as the incident angles are varied, i.e. the sensor rotates with the sample and is therefore maintained in the same position relative to the sample-based coordinate system as both incident beam angles are changed.

Coupled directly to rotation stage (B) is rotation stage (C) for changing the sensor azimuth angle. This stage has a hole through its center to allow the sample post to come directly out from the center of stage (B). Finally, mounted on the sensor azimuth stage (C) is an arc (D) on one end of which the sensor is mounted. This arc can be moved through 90° to change the sensor polar angle.

For convenience and to speed alignment, stage (A) is mounted on an X–Y positioner, stage (B) is mounted on a vertical positioner. Also, the sample is held in an adjustable-height post holder to accommodate different-thickness samples and to allow retraction of the sample for direct sensor calibration and measurement of the incident beam intensity.

The detection system

The detection system consists of a chopper to modulate the incident beam, a photodiode, a lock-in amplifier, and a computer used both for control of the lock-in amplifier and to record data as they are collected. For purposes of discussion, the system is considered in two parts: the sensor and the amplifier.

Although many previously reported experimental results were based on the use of a photomultiplier tube (PMT), the current device uses a photodiode operating in the photovoltaic mode. This decision was based on the desire to keep the entire system as simple as possible. Photodiodes are much easier to work with than PMTs. They have a large range over which their output is linear in response to intensity; in the photovoltaic mode they are linear over approximately five orders of magnitude. Also, when operated in the photovoltaic mode, no additional circuitry except a load resistor is required. If a larger range were needed, the next step would be to apply a bias voltage to the photodiode and operate it in the photoconductive mode. Only if much greater sensitivity were required would switching to a PMT be recommended.

The question of relative sensor size, sample size and source beam diameter typically requires that some compromises be made. As described by Nicodemus [11], there are two practical approaches to the geometric relationship between source, sample, and sensor size. First, the incident beam (source) can have a small area, in which case the sample and sensor must have areas large enough to encompass the entire beam at the largest incident polar angle to be used. Alternatively, the sample and sensor can be small, in which case the incident beam must be bigger than the area on the sample from which the sensor receives radiation. A variation of the latter is used in this apparatus; a circular sample is used with an incident beam and sensor of the same diameter.

In the case of the first approach, a laser beam of approximately 2 mm diameter was directed at the sample. The sensor, a 10 mm^2 circular photodiode, was just large enough to accept the entire beam. Although a larger sensor would be desirable, this was adequate for evaluation of the large area approach. Several operational features associated with this approach quickly became apparent:

(1) When the sensor area is large relative to the incident beam diameter, the fact that the incident beam intensity may have a non-uniform distribution is irrelevant. This allows direct use of a laser beam.

(2) Even with the lowest-power laser available, a 0.5 mW He–Ne laser, the total intensity was so high that without either biasing the photodiode or using an intensity reducing neutral density filter, the sensor was far out of its linear range.

(3) In the specific case used to test this approach, the 2 mm diameter incident beam from a He–Ne laser displayed an intensity distribution that was approximately gaussian in shape. With the 10 mm^2 photodiode area, the limit for the incident beam polar angle was 56°. At greater angles, the sensor would not 'see' the entire incident beam.

(4) With the large area of the sensor, additional precautions were required to limit detection to the signal of interest. It was observed that unless the ambient light levels were low or the source beam path was carefully shielded, the detection system would be very limited in its low-level capabilities. This was because ambient light was traveling through the chopper and being reflected to the sensor; no signal smaller than that caused by ambient light could be detected. Overall, use of the small beam–large sensor approach resulted in a reduced sensitivity of the detection system of approximately two orders of magnitude.

The second approach, using a sensor with a small acceptance angle, was tested using the same 10 mm^2 photodiode, but with a series of baffles in the sensor housing to restrict the acceptance angle to a solid angle of approximately 0.00084 sr. This arrangement

was superior to the large sensor for our purposes but was not entirely without problems:

(1) When the sensor area is small relative to the incident beam diameter, the fact that the incident beam intensity may have a non-uniform distribution is increasingly important as the reflectance polar angle increases. When this angle is small, the sensor sees a nearly uniform intensity beam because of its narrow acceptance angle. However, when it is large, the sensor sees a larger portion of the irradiated area on the sample. If non-uniformities exist in the incident beam intensity, the incident intensity used for normalizing the reflectance changes as the incident polar angle changes.

(2) Also a consideration when using a small-area sensor is that the small area of the sensor opening results in very low intensity at the photodiode. For the source used in these measurements, this was advantageous because it put intensity in a range where a linear output could be expected from a photodiode operated in the photovoltaic mode.

(3) An additional feature associated with the small-area sensor opening is its sensitivity to spatially abrupt changes in intensity. The output of this sensor changes dramatically with very small changes in position when the beam incident on the sensor is sharp edged, as in a specular reflection. With the geometry of this apparatus, the ability of the sensor to resolve the location of intensity peaks is about 0.22°; this clearly exceeds the 0.5° resolution of the goniometer.

In both cases, the sensor was mounted on top of the goniometer arm. As can be seen in Fig. 2, this arm is below the azimuthal axes of rotation so that when the sensor is mounted on the arm surface, the sensor axis is coincident with the other three goniometer axes as well as the axis of the incident beam. Having the arm offset from the axis of rotation allows the incident beam to reach the sample for all goniometer positions except for a small cone around the incident beam.

The direct current output of the sensor is modulated by the chopper and fed directly to a lock-in amplifier. The reference frequency generated by the chopper is an input to the amplifier. Because the signal of interest (the photodiode output) is being modulated at a precisely known frequency, the lock-in is able to act as a filter with a very narrow bandwidth. When coupled with a high gain amplifier, the result is an ability to amplify and extract signals that are below the ambient noise level. In this particular case, even though the output of the photodiode was in the nanovolt range, use of the lock-in amplifier allowed work to be conducted in ambient light conditions. The only constraint resulting from the use of a lock-in under these conditions is that the time constants required for accurate readings can result in periods on the order of minutes for each data point.

ALIGNMENT AND CALIBRATION

Care in alignment of the reflectometer is essential; the uncertainty associated with angular position is directly dependent on the accuracy of alignment. Because the goniometer allows independent selection of each of the incident beam angles and each of the reflected beam angles, the four axes about which rotation may take place must be aligned. In addition, the incident beam axis and the sensor axis must also be aligned.

The first step in alignment was to establish the orientation of the incident beam such that it was parallel to the optical table surface. Then, in order, the axes of rotation for stages A, B and C were aligned to be (a) coincident at a point defined by the intersection of the incident beam and the sample surface and (b) either perpendicular to or coincident with the incident beam as appropriate. This procedure required iteration, and when complete a 0.1 mm diameter incident beam would remain at a constant location for any rotation of stages B and C, and the same incident beam would grow symmetrically as stage A was rotated. Alignment of the sensor polar axis was accomplished through inserting a pointer through the sensor holder with the tip located at the sample surface. Movement of the pointer tip relative to the incident beam on the sample surface as stage D was rotated indicated the alignment of the sensor axis. It is worth noting that when originally bolted together, the positioning accuracy of the system was within $\pm 1°$ for all of the incident and reflected beam directions. The tedious and time consuming procedure of detailed alignment is necessary both to maximize accuracy and to have a quantitative basis for estimating uncertainties.

Calibration of the angular position indicators is required to ensure that the readout on the goniometer provides an accurate indication of the angles to which it is set. This was accomplished as a part of the alignment procedure.

Calibration of the intensity measurement system is also required. This was accomplished by calibrating the sensor using neutral density filters. Although an absolute measurement of intensities could be made, it is acceptable to calibrate the sensor in terms of a percent of incident intensity because reflectance is defined as a ratio of reflected to incident intensity. To accomplish this, the sample was retracted out of the way and the sensor was rotated to receive light directly from the source. Calibrated neutral density filters were placed in the incident beam to reduce the intensity by known amounts. As expected, the output of the photodiode was almost exactly linear with respect to the intensity incident on the photodiode.

Several other tests were performed to experimentally confirm sensor characteristics: (1) the entire source and detection system was tested for drift over time; (2) using the beam from a low-power laser, the edge detection abilities of the sensor were determined by traversing the sensor across the beam and (3) as a check on the acceptance angle for the directional sensor, the sensor was lined up with the beam and then rotated with respect to the sensor front plane.

The latter two tests confirmed estimates based on the nominal geometry of the sensor components.

UNCERTAINTY OF MEASUREMENTS

When data are to be used in validating a numerical code, having a clear understanding of the associated uncertainty is essential. The results of bi-directional reflectance measurements are reported in terms of two types of quantities: the angles that define position of the incident and reflected beams, and the ratio of intensities that define bi-directional reflectance. By virtue of the goniometer design, uncertainties associated with each of the four direction defining angles are independent. For each of these angles, the uncertainty for the manually operated system is $\pm 0.25°$.

Uncertainty of the calculated reflectance is determined in the standard fashion [12]:

$$\omega(f) = \left\{\left(\frac{\partial f}{\partial x_1}\omega_{x1}\right)^2 + \left(\frac{\partial f}{\partial x_2}\omega_{x2}\right)^2 + \cdots\right\}^{1/2} \quad (3)$$

where in this case the function f is given by:

$$f(\theta_i, \phi_i, \theta_r, \phi_r) = \frac{i_{r,\lambda}(\theta_i, \phi_i, \theta_r, \phi_r)}{q_o \cos(\theta_i)} \quad (4a)$$

or, recalling that the ratio of measured intensity to measured incident flux is the same as the ratio of the voltages output from the linear photodiode:

$$f(\theta_i, \phi_i, \theta_r, \phi_r) = \frac{V_r(\theta_i, \phi_i, \theta_r, \phi_r)}{V_i \cos(\theta_i)}. \quad (4b)$$

For this apparatus the range of uncertainty for the variables in bi-directional reflectance was as follows:

V_r: uncertainty = 0.0001*full Scale (range from 1 nV to 1000 nV)

V_i: uncertainty = 0.0001*full Scale (typically 1000 nV)

angles: uncertainty = 0.25° (0.005 rad).

The nature of the definition of BRDF ensures that overall uncertainty for measurements will range from some finite value to a very large value as the cosine term in the denominator goes from 1 to a very small value. Excluding the effects of this term, uncertainty for the measurements described in the next section was always less than 2%.

SAMPLE DATA

A number of materials have been tested using this reflectometer. As described in the introduction, bi-directional reflectance data are necessarily voluminous in nature. Therefore, only a portion of the results for a common flat-white paint are included in this paper. These results have been selected to demonstrate the importance of considering full bi-directional reflectance data when modeling common types of materials.

All of the bi-directional reflectance data shown is for Krylon Flat-White paint (no. 1502). Two coats of the paint were applied to a smooth (600 grit) aluminum substrate. The incident beam was from a He–Ne laser operating at 632.8 nm with random polarization. The sensor diameter was 10 mm. The example bi-directional reflectance data are shown in Fig. 3. It is clear in this plot that the paint is mostly diffuse for angles of incidence less than about 45°, but that reflection becomes increasingly specular as the incident polar angle increases above that value. The conclusion to be drawn is that if these circumstances will occur in a situation where multiple reflections are likely, the model used for analysis should not ignore the change in specularity of reflection as a function of incident angle.

CONCLUSIONS

An apparatus for the measurement of bi-directional reflectance has been described in detail. The key features that set it apart from previous work are: (1) direct reading of all angles involved, (2) nearly complete hemispheric coverage, (3) the ability to measure incident flux directly with the same sensor as used for reflected flux, (4) a goniometer that moves the sample and sensor about all four axis therefore providing great flexibility in the source used for the incident beam, (5) linear response over five orders of magnitude in intensity and (6) a minimum of custom machining (only one axis requires a custom machined stage). The opportunities for improvement fall into the categories of operational improvements and accuracy improvements.

All of the operational improvements relate to further automation of the data collection process. Specifically, each axis of rotation could be motorized and the existing computer program for data acquisition could be extended to include control of the goniometer motion. Improvements in accuracy can be achieved by improving the quality of the source beam both in terms of uniformity and stability, by using a more precise method of measuring the area of the sensor and its distance from the sample, and by increasing the resolution of the scales used on the goniometer.

This reflectometer has been used to evaluate the bi-directional reflectance of several types of common engineering materials. It is clear that for some materials the traditional practice of assuming azimuthal symmetry, and perhaps even the practice of modeling reflectance as a linear combination of specular and diffuse components, needs to be re-evaluated in light of the common availability of computational resources with the power to complete numerical analysis without those simplifications.

Acknowledgements—This work was supported by the Engineering Research Program, Division of Basic Energy Sciences of the U.S. Department of Energy under grant no. F67991ER14171.

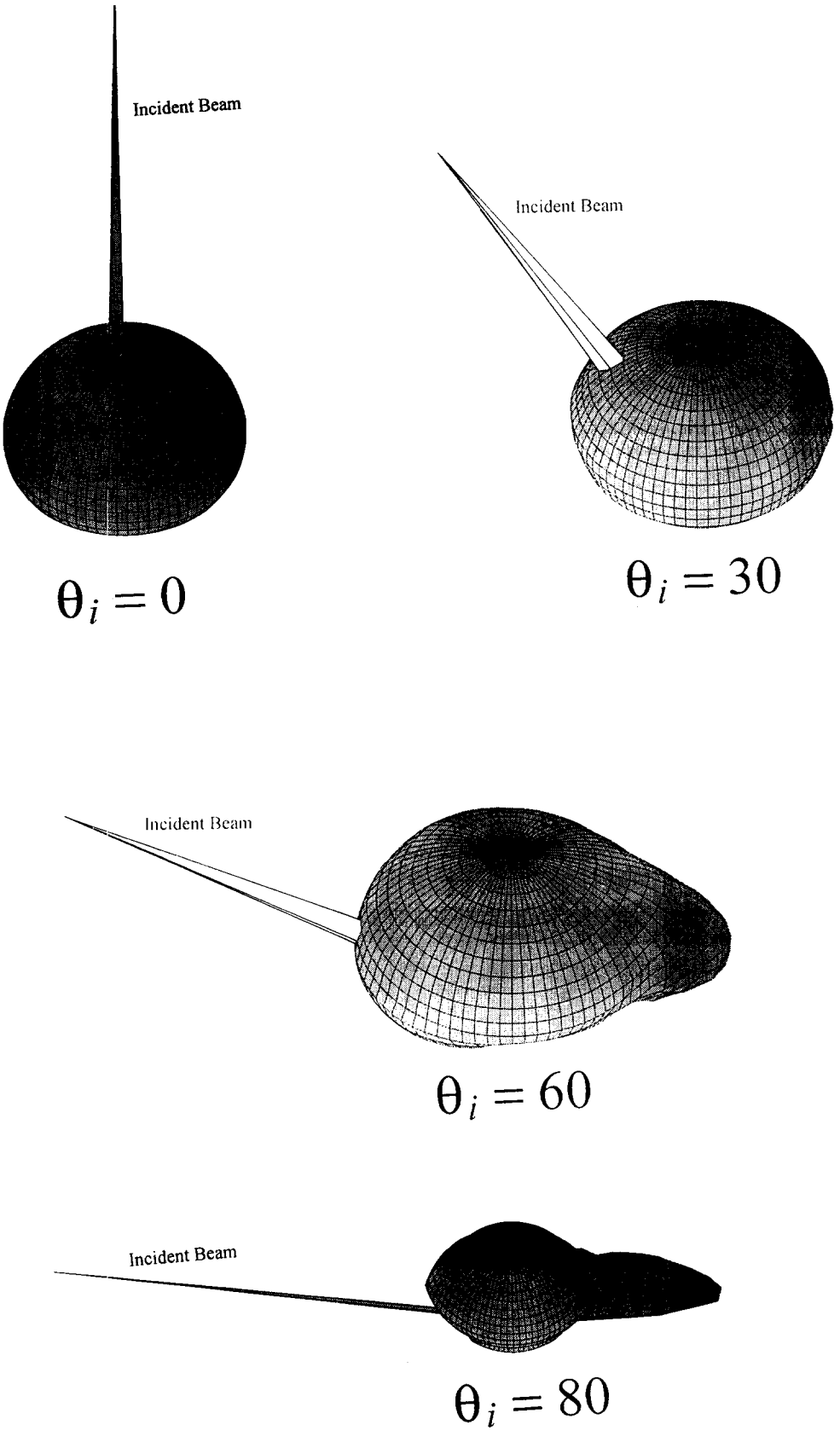

Fig. 3. Plots of the bidirectional reflectance for Krylon flat white paint (no. 1502) for four incident polar angles. The plots are of log(BRDF) and the incident intensities are shown to scale.

REFERENCES

1. J. C. Richmond and J. J. Hsia, Bi-directional reflectometry—II. Bibliography on scattering by reflection from surfaces, *J. Res. NBS (Phys. Chem.)* **80A**(2), 207–220 (1976).
2. Y. S. Touloukian, D. P. DeWitt and R. S. Hernicz (Eds), *Thermal Radiative Properties: Coatings* In *Thermophysical Properties of Matter*, Vol. 9. Plenum Press, New York (1970).
3. M. Q. Brewster, *Thermal Radiative Transfer and Properties*. John Wiley, New York (1992).
4. C. F. Bohren and D. R. Huffman, *Absorption and Scattering of Light by Small Particles*. John Wiley, New York (1983).
5. R. Siegel and J. R. Howell, *Thermal Radiation Heat Transfer*. McGraw-Hill, New York (1972).
6. M. F. Modest, *Radiative Heat Transfer* (1st Edn). McGraw-Hill, New York (1993).
7. A. A. De Silva and B. W. Jones, Bi-directional spectral reflectance and directional–hemispherical spectral reflectance of six materials used as absorbers of solar energy, *Solar Energy Mater.* **15**(5), 391–401 (1987).
8. E. R. Miller, and R. S. Vun Kannon, Development and use of a bi-directional spectroreflectometer, *Progr. Aeron. Astron.* **20,** 219–233 (1967).
9. J. J. Hsia and J. C. Richmond, Bi-directional reflectometry—I. A high resolution laser bi-directional reflectometer with results on several optical coatings, *J. Res. NBS (Phys. Chem.)* **80A**(2), 189–205 (1976).
10. G. M. Keating and J. A. Mullins, Vectorial Reflectance of the Explorer IX Satellite Material, NASA TN-D-2388 (August 1964).
11. F. E. Nicodemus, J. C. Richmond and J. J. Hsia, *Geometrical considerations and Nomenclature for Reflectance*, pp. 1–52. NBS Monograph (October 1977).
12. J. P. Holman, *Experimental Methods for Engineers* (3rd Edn). McGraw Hill, New York (1978).
13. M. K. Drost and J. R. Welty, Monte-Carlo simulation of radiation heat transfer in arrays of fixed discrete surfaces using cell-to-cell photon transport, *Proceedings of the 28th National Heat Transfer Conference*, ASME, San Diego, California (1991).